
α -SSC: Uncertainty-Aware Camera-based 3D Semantic Scene Completion

Sanbao Su

University of Connecticut
sanbao.su@uconn.edu

Nuo Chen

New York University
nc3144@nyu.edu

Felix Juefei-Xu

New York University
juefei.xu@nyu.edu

Chen Feng

New York University
cfeng@nyu.edu

Fei Miao

University of Connecticut
fei.miao@uconn.edu

Abstract

In the realm of autonomous vehicle (AV) perception, comprehending 3D scenes is paramount for tasks such as planning and mapping. Semantic scene completion (SSC) aims to infer scene geometry and semantics from limited observations. While camera-based SSC has gained popularity due to affordability and rich visual cues, existing methods often neglect the inherent uncertainty in models. To address this, we propose an uncertainty-aware camera-based 3D semantic scene completion method (α -SSC). Our approach includes an uncertainty propagation framework from depth models (Depth-UP) to enhance geometry completion (up to 11.58% improvement) and semantic segmentation (up to 14.61% improvement). Additionally, we propose a hierarchical conformal prediction (HCP) method to quantify SSC uncertainty, effectively addressing high-level class imbalance in SSC datasets. On the geometry level, we present a novel KL divergence-based score function that significantly improves the occupied recall of safety-critical classes (45% improvement) with minimal performance overhead (3.4% reduction). For uncertainty quantification, we demonstrate the ability to achieve smaller prediction set sizes while maintaining a defined coverage guarantee. Compared with baselines, it achieves up to 85% reduction in set sizes. Our contributions collectively signify significant advancements in SSC accuracy and robustness, marking a noteworthy step forward in autonomous perception systems.

1 Introduction

Achieving a comprehensive understanding of 3D scenes holds paramount importance for subsequent tasks such as planning and map construction (Wang and Huang [2021]). Semantic scene completion (SSC) emerges as a solution that jointly infers the geometry completion and semantic segmentation from limited observations (Song et al. [2017], Hu et al. [2023]). SSC approaches typically fall into two categories based on the sensors they utilize: LiDAR-based SSC (LSSC) and Camera-based SSC (CSSC). While LiDAR sensors offer precise depth information (Roldao et al. [2020], Cheng et al. [2021]), they are costly and less portable. Conversely, cameras, with their affordability and ability to capture rich visual cues of driving scenes, have gained significant attention (Cao and De Charette [2022], Li et al. [2023b], Tian et al. [2024], Zhang et al. [2023]). For CSSC, the depth prediction is essential for the accurate 3D reconstruction of scenes. However, existing methodologies often ignore errors inherited from depth models in the real-world scenarios (Poggi et al. [2020]). Moreover, how to utilize the propagated depth uncertainty information and rigorously quantify the uncertainty of

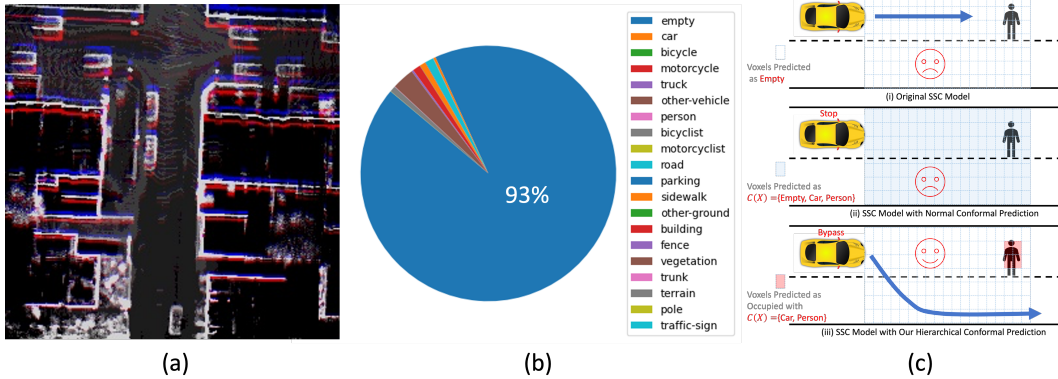


Figure 1: (a): Example: influence of depth estimation error on the geometry completion of SSC in bird’s-eye view. The ground truth is delineated by white lines, paralleled with estimations with $\pm 0.2m$ depth estimation errors denoted by blue and red lines. (b): The class distribution within the SemanticKITTI validation dataset, showing a significant class imbalance: 93% empty voxels, while person voxels, crucial for safety, are a mere 0.7%. (c): AV planning example with one SSC model as perception input. (i) The original SSC model predicts the voxels at the person’s location as empty due to high-level class imbalance in (b), causes the vehicle to go straight and be unsafe to the person. (ii) With conformal prediction in the literature (Angelopoulos and Bates [2021]), the SSC model makes the prediction sets of all voxels contain nonempty classes, the vehicle stops far away from the person. (iii) Our hierarchical conformal prediction will firstly only predict the voxels at the location of the person as occupied, since it improves the occupied recall of the rare safety-critical class (person). Then it will generate the prediction sets for predicted occupied voxels, which contain car and person classes. With the above perception input, the vehicle will avoid collision with the person.

the final SSC outputs, especially when there exists high-level class imbalance as observed in SSC datasets, remains challenging and unexplored.

We explain the importance of considering depth uncertainty propagation and SSC uncertainty quantification in Fig. 1. The influence of depth estimation errors on the geometry completion of CSSC is shown in (a), with the ground truth delineated by white lines, and estimations with $\pm 0.2m$ depth estimation errors in blue and red lines. Errors in depth estimation significantly reduce the performance of geometry completion, especially in distant regions. In this paper, we propose a novel uncertainty propagation framework from depth models (Depth-UP) to improve the performance of CSSC models.

The datasets utilized in SSC tasks often exhibit a pronounced class imbalance, with empty voxels comprising a significant proportion illustrated in Fig. 1 (b) of the widely used SemanticKITTI (Behley et al. [2019]). Empty voxels constitute a staggering 93% while person voxels, crucial for safety, are a mere 0.7%. Consequently, neural networks trained on such imbalanced data, coupled with maximum a-posterior classification, may inadvertently disregard classes that are infrequent in occurrence within the dataset (Tian et al. [2020]). This leads to reduced accuracy and recall for rare classes such as person. However, for safety-critical systems such as autonomous vehicles (AV), ensuring occupied recall for rare classes is imperative to prevent potential collisions and accidents (Chan et al. [2019]). Fig. 1 (c).i shows a driving scenario where the AV cannot identify the person and hit the person, when an SSC model predicts the person as empty voxels. Hence, to enhance planning safety, SSC systems should ideally provide uncertainty quantification for their predictions (Liang et al. [2021]). If we apply a commonly used conformal prediction Angelopoulos and Bates [2021] method on SSC models, the vehicle will stop far away from the person as shown in Fig. 1 (c).ii. Because the model predicts the prediction sets of all voxels in front of the vehicle containing nonempty classes.

To address these dual requirements, we propose a hierarchical conformal prediction (HCP) method that improves the occupied recall of rare classes for geometry completion while generating prediction sets for predicted occupied voxels with class coverage guarantees for semantic segmentation. Fig. 1 (c).iii shows that our HCP improves the occupied recall of the rare safety-critical class (person), so the SSC model only predicts the voxels on the location of the person as occupied. HCP will also generate the prediction sets for predicted occupied voxels, containing car and person classes. With the above perception input, the vehicle will avoid collision with the person.

Through extensive experiments on VoxFormer (Li et al. [2023b]) and two datasets, we show that our Depth-UP achieves up to 11.58% increase in geometry completion and 14.61% increase in semantic segmentation. Our HCP achieves 45% improvement in the geometry prediction for the person class, with only 3.4% total IoU overhead. This improves the prediction of rare safety-critical classes, such as persons and bicyclists, thereby reducing potential risks for AVs. And compared with baselines, our HCP reduces up to 85% set sizes and up to 91% coverage gap. These results highlight the significant improvements in both accuracy and uncertainty quantification offered by our α -SSC approach.

Our contributions can be summarized as follows:

1. To address the challenging camera-based 3D Semantic Scene Completions (SSCs) problem for autonomous driving, we recognize the problem from a fresh uncertainty quantification (UQ) perspective. More specifically, we propose the uncertainty-aware camera-based 3D semantic scene completion method (α -SSC), which contains the uncertainty propagation from depth models (Depth-UP) to improve SSC performance by utilizing uncertainty information and our novel hierarchical conformal prediction (HCP) method to quantify the uncertainty of SSC.
2. To the best of our knowledge, we are the first attempt to propose Depth-UP to improve the SSC performance, where the direct modeling quantifies the uncertainty of depth estimation and the uncertainty is utilized on both geometry completion and semantic segmentation. This leads to a solid improvement in common SSC models.
3. To solve the high-level class imbalance challenge on SSC, which results in biased prediction and reduced recall for rare classes, we propose the HCP. On geometry completion, a novel KL-based score function is proposed to improve the occupied recall of safety-critical classes with little performance overhead. On the semantic segmentation, we achieve a smaller prediction set size under the defined class coverage guarantee. Overall, the proposed α -SSC, combined with Depth-UP and HCP, has shown that UQ is an integral and vital part of CSSC tasks, with an extendability over to a broader set of 3D scene understanding tasks that go beyond the AV perception.

2 Related Work

Semantic Scene Completion. The concept of 3D Semantic Scene Completion (SSC) was first introduced by SSCNet (Song et al. [2017]), integrating both geometric and semantic reasoning. Since its inception, numerous studies have emerged, categorized into two streams: LiDAR-based SSC (Roldao et al. [2020], Cheng et al. [2021], Yan et al. [2021]) and Camera-based SSC (CSSC) (Cao and De Charette [2022], Li et al. [2023b], Tian et al. [2024], Zhang et al. [2023]). CSSC has gained increasing attention owing to cameras’ advantages in visual recognition and cost-effectiveness. Depth predictions are instrumental in projecting 2D information into 3D space for CSSC tasks. Existing methodologies generate query proposals using depth estimates and leverage them to extract rich visual features from the 3D scene. However, these methods overlook depth estimation uncertainty. In this work, we propose an uncertainty propagation framework from depth models to enhance the performance of CSSC models.

Uncertainty Quantification and Propagation. Uncertainty quantification (UQ) holds paramount importance in ensuring the safety and reliability of autonomous systems such as robots (Jasour and Williams [2019]) and AVs (Meyer and Thakurdesai [2020]). Moreover, UQ for perception tasks can significantly enhance the planning and control processes for safety-critical autonomous systems (Xu et al. [2014], He et al. [2023]). Different types of UQ methods have been proposed. Monte-Carlo dropout (Miller et al. [2018]) and deep ensemble (Lakshminarayanan et al. [2017]) methods require multiple runs of inference, which makes them infeasible for real-time UQ tasks. In contrast, direct modeling approaches (Feng et al. [2021]) can estimate uncertainty in a single inference pass in real-time perception. While UP frameworks from depth to 3D object detection have demonstrated efficacy in enhancing accuracy (Lu et al. [2021], Wang et al. [2023]), no prior works have addressed UP from depth to 3D CSSC. This paper aims to bridge this gap by proposing a novel approach to UP in this context, and we design a depth uncertainty propagation (UP) module called Depth-UP based on direct modeling. Conformal prediction can construct statistically guaranteed uncertainty sets for model predictions (Angelopoulos and Bates [2021]), however, there is limited CP literature for highly class-imbalanced tasks, rare but safety-critical classes (e.g., person) remains challenging for SCC models. Hence, we develop a hierarchical conformal prediction method to quantify uncertainties of the output of SSC tasks characterized by highly imbalanced-class.

3 Method

We design a novel uncertainty-aware camera-based 3D semantic scene completion method (α -SSC), which contains the uncertainty propagation from depth models to SSC (Depth-UP) to improve performance of SSC and the hierarchical conformal prediction (HCP) to quantify the uncertainty of SSC. Figure 2 presents the methodology overview. The major novelties are: (1) Depth-UP quantifies the uncertainty of depth estimation by direct modeling (DM) and then propagates it through depth feature extraction (for semantic segmentation) and building a probabilistic voxel grid map by probabilistic geometry projection (for geometry completion). (2) Our HCP calibrates the probability outputs of the SSC model on the geometry and semantic levels. First, it predicts the voxel’s occupied state by the quantile on the novel KL-based score function as Eq. 6, which can improve the occupied recall of rare safety-critical classes with a small performance overhead under the high-level class imbalance situation. Then it generates prediction sets for these predicted occupied voxels, which achieve a better coverage guarantee and smaller sizes of prediction sets.

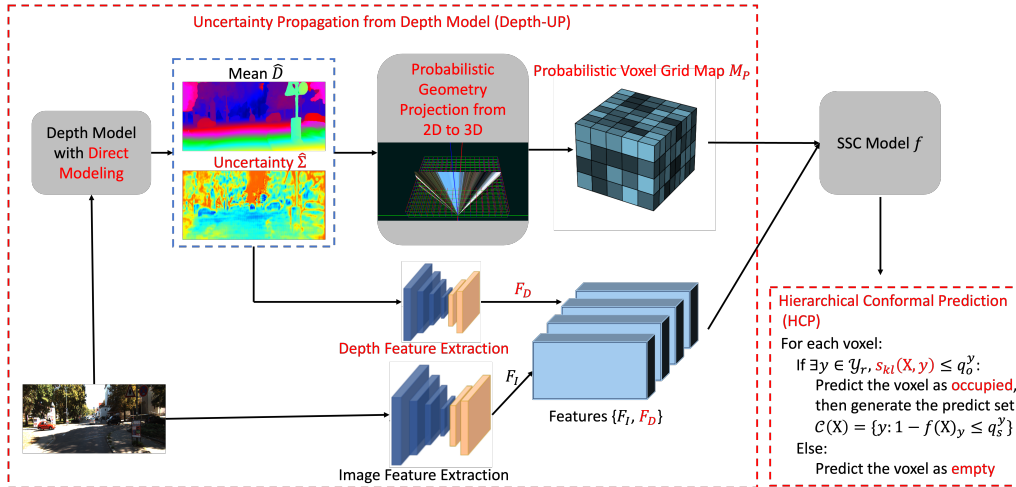


Figure 2: Overview of our α -SSC method. The red color highlights the novelties and important techniques in our method. In the Depth-UP part, we calculate the uncertainty of depth estimation through direct modeling. Then we propagate it through depth feature extraction (for semantic segmentation) and building a probabilistic voxel grid map by probabilistic geometry projection (for geometry completion). In the HCP, we predict voxels’ occupied state by the quantile on the novel KL-based score as Eq. 6, which can improve occupied recall of rare classes, and then only generate prediction sets for these predicted occupied voxels.

3.1 Preliminary

Camera-based Semantic Scene Completion (CSSC) predicts a dense semantic scene within a defined volume in front of the vehicle solely from RGB images (Cao and De Charette [2022]). Specifically, with an input image denoted by $\mathbf{X} \in \mathbb{R}^{3 \times H \times W}$, one CSSC model first extracts 2D image features \mathbf{F}_I using backbone networks like ResNet (He et al. [2016]) and estimates the depth value for each pixel, denoted by $\hat{\mathbf{D}} \in \mathbb{R}^{H \times W}$, employing depth models such as monocular depth estimation (Bhat et al. [2021]) or stereo depth estimation (Shamsafar et al. [2022]). Subsequently, the model generates a probability voxel grid $\hat{\mathbf{Y}} \in [0, 1]^{M \times U \times V \times D}$ based on \mathbf{F}_I and $\hat{\mathbf{D}}$, assigning each voxel to the class with the highest probability. Each voxel within the grid is categorized as either empty or occupied by a specific semantic class. The ground truth voxel grid is denoted as \mathbf{Y} . Here, H and W signify the height and width of the input image, while U , V and D represent the height, width, and length of the voxel grid, M denotes the total number of relevant classes (including the empty class), respectively.

3.2 Uncertainty Propagation Framework (Depth-UP)

In contemporary CSSC methods, the utilization of depth models has been pivotal in facilitating the projection from 2D to 3D space, primarily focusing on geometric aspects. Nonetheless, these approaches often overlook the inherent uncertainty associated with depth prediction. Recognizing the potential to enhance CSSC performance by harnessing this uncertainty, we introduce a novel

framework centered on uncertainty propagation from depth models to CSSC models (Depth-UP). Our approach involves quantifying the uncertainty inherent in depth models through a direct modeling (DM) method (Su et al. [2023], Feng et al. [2021]) and integrating this uncertainty information into both geometry completion and semantic segmentation of CSSC to improve the final performance.

Direct Modeling (DM). Depth-UP includes a DM technique (Su et al. [2023], Feng et al. [2021]) to infer the standard deviation associated with the estimated depth value of each pixel in the image, with little time overhead. An additional regression header, with a comparable structure as the original regression header for $\hat{\mathbf{D}}$, is tailored to predict the standard deviation $\hat{\Sigma}$. Subsequently, this header is retrained based on the pre-trained deep model. We assume that the estimated depth value is represented as a single-variate Gaussian distribution, and the ground truth depth follows a Dirac delta function (Arfken et al. [2011]). For the retraining process, we define a regression loss function as the Kullback-Leibler (KL) divergence between a single-variate Gaussian distribution and a Dirac delta function (Murphy [2012]), where $\mathbf{D} \in \mathbb{R}^{H \times W}$ is the ground-truth depth matrix for the image:

$$\mathcal{L}_{KL}(\mathbf{D}, \hat{\mathbf{D}}, \hat{\Sigma}) = \frac{1}{HW} \sum_{i=1}^H \sum_{j=1}^W \frac{(d_{ij} - \hat{d}_{ij})^2}{2\hat{\sigma}_{ij}^2} + \log |\hat{\sigma}_{ij}|. \quad (1)$$

Propagation on Geometry Completion. Depth information is used to generate the 3D voxels on geometry in CSSC. There are two key challenges inherent: occupied probability estimation for each voxel and lens distortion during geometric transformations. Existing SSC models, such as VoxFormer (Li et al. [2023b]), solves the lens distortion by projecting the depth information into a 3D point cloud, and then generating the binary voxel grid map $\mathbf{M}_b \in \{0, 1\}^{U \times V \times D}$, where each voxel is marked as 1 if occupied by at least one point. However, they ignore the uncertainty of depth. Here we propagate the depth uncertainty into the geometry of CSSC by solving the above two challenges.

Our Depth-UP generates a **probabilistic voxel grid map** $\mathbf{M}_p \in [0, 1]^{U \times V \times D}$ that considers both the lens distortion and the uncertainty in depth estimation, with $\{\hat{\mathbf{D}}, \hat{\Sigma}\}$ from DM. For pixel (h, w) , the estimated depth mean is \hat{d}_{hw} , we project it into the point (x, y, z) in 3D space:

$$x = \frac{(h - c_h) \times z}{f_u}, y = \frac{(w - c_w) \times z}{f_v}, z = \hat{d}_{hw} \quad (2)$$

When the estimated depth follows a single-variate Gaussian distribution with a standard deviation $\hat{\sigma}_{hw}$, the location of the point may be on any position along a ray started from the camera. It is difficult to get the exact location of the point, but we can estimate the probability of the point in one voxel (u, v, d) . So for one voxel (u, v, d) , we compute its probability of being occupied by points:

$$\mathbf{M}_p(u, v, d) = \min \left(1, \sum_{\rho_{hw} \in \Psi_{uvd}} \int_{z_s}^{z_e} \mathcal{N}(z | \hat{d}_{hw}, \hat{\sigma}_{hw}^2) dz \right) \quad (3)$$

where Ψ_{uvd} is the set of rays starting from the camera and passing the voxel (u, v, d) . For ray ρ_{hw} corresponding to the pixel (h, w) , we compute the cumulative probability between the two crosspoints with the voxel. The corresponding depth value of the two crosspoints are z_s and z_e . The probabilistic voxel grid map $\mathbf{M}_p \in [0, 1]^{U \times V \times D}$ replaces the original binary voxel grid map.

Propagation on Semantic Segmentation. The extraction of 2D features \mathbf{F}_I from the input image has been a cornerstone for CSSCs to encapsulate semantic information. However, harnessing the depth uncertainty information on the semantic features is ignored. Here by augmenting the architecture with an additional ResNet-18 backbone (He et al. [2016]), we extract depth features \mathbf{F}_D from the estimated depth mean and standard deviation $\{\hat{\mathbf{D}}, \hat{\Sigma}\}$. These newly acquired depth features are then seamlessly integrated with the original 2D features, constituting a novel set of input features $\{\mathbf{F}_I, \mathbf{F}_D\}$ as shown in Fig. 2. This integration strategy capitalizes on the wealth of insights garnered from prior depth predictions, thereby enhancing the CSSC process with refined semantic understanding.

3.3 Hierarchical Conformal Prediction (HCP)

3.3.1 Preliminary

Standard Conformal Prediction. For classification, conformal prediction (CP) (Angelopoulos and Bates [2021], Ding et al. [2024]) is a statistical method to post-process any models by producing

the set of predictions and uncertainty quantification (UQ) with theoretically guaranteed marginal coverage of the correct class. With M classes, consider the calibration data $(\mathbf{X}_1, \mathbf{Y}_1), \dots, (\mathbf{X}_N, \mathbf{Y}_N)$ with N data points that are never seen during training, the standard CP (SCP) includes the following steps: (1) Define the score function $s(\mathbf{X}, y) \in \mathbb{R}$. (Smaller scores encode better agreement between \mathbf{X} , and y). The score function is a vital component of CP. A typical score function of a classifier f is $s(\mathbf{X}, y) = 1 - f(\mathbf{X})_y$, where $f(\mathbf{X})_y$ represents the y^{th} softmax output of $f(\mathbf{X})$. (2) Compute q as the $\frac{\lceil (N+1)(1-\alpha) \rceil}{N}$ quantile of the calibration scores, where $\alpha \in [0, 1]$ is a user-chosen error rate. (3) Use this quantile to form the prediction set $\mathcal{C}(\mathbf{X}_{test}) \subset \{1, \dots, M\}$ for one new example \mathbf{X}_{test} (from the same distribution of the calibration data): $\mathcal{C}(\mathbf{X}_{test}) = \{y : s(\mathbf{X}_{test}, y) \leq q\}$. The SCP provides a coverage guarantee that $\mathbb{P}(\mathbf{Y}_{test} \in \mathcal{C}(\mathbf{X}_{test})) \geq 1 - \alpha$.

Class-Conditional Conformal Prediction. The SCP achieves the marginal guarantee but may neglect the coverage of some classes, especially on class-imbalanced datasets (Angelopoulos and Bates [2021]). Class-Conditional Conformal Prediction (CCCP) targets class-balanced coverage:

$$\mathbb{P}(\mathbf{Y}_{test} \in \mathcal{C}(\mathbf{X}_{test}) | \mathbf{Y}_{test} = y) \geq 1 - \alpha^y, \quad (4)$$

for $\forall y \in \{1, \dots, M\}$. It means every class y has at least $1 - \alpha^y$ probability of being included in the prediction set when the label is y . Hence, the prediction sets satisfying Eq. 4 are effectively fair with respect to all classes, even the very rare ones.

3.3.2 Our Hierarchical Conformal Prediction

Algorithm 1: Our Hierarchical Conformal Prediction (HCP)

Data: number of classes is M which include empty, labeled calibration dataset $\mathcal{D}_{cali}(\mathbf{X}, \mathbf{Y})$ with N samples, unlabeled test dataset $\mathcal{D}_{test}(\mathbf{X})$ with T samples, the considered rare class set \mathcal{Y}_r , the corresponding occupied error rate α_o^y for $\forall y \in \mathcal{Y}_r$, defined class-specific error rate α^y for $\forall y \in \mathcal{Y} \setminus \{1\}$, the SSC model f .

Result: Prediction set $\mathcal{C}(\mathbf{X}_i)$ for $\forall \mathbf{X}_i \in \mathcal{D}_{test}$

```

1 /* Calibration Step: Geometric Level */
2  $\mathcal{S}^y = \emptyset$  for  $\forall y \in \mathcal{Y}_r$ ;  $\mathbf{O} = \{\varepsilon, 1, \dots, 1\}^M$ ;
3 for  $(\mathbf{X}_i, \mathbf{Y}_i) \in \mathcal{D}_{cali}$  do
4   |  $s_{kl}(\mathbf{X}, y) = D_{kl}(f(\mathbf{X}_i) || \hat{\mathbf{O}})$ , for  $y = \mathbf{Y}_i \in \mathcal{Y}_r$  as Eq. 6; add  $s_{kl}(\mathbf{X}, y)$  into  $\mathcal{S}^y$ ;
5 end
6  $q_o^y = \text{Quantile}(\frac{\lceil (N_y+1)(1-\alpha_o^y) \rceil}{N_y}, \mathcal{S}^y)$  where  $N_y = |\mathcal{S}^y|$ , for  $\forall y \in \mathcal{Y}_r$ ;
7 /* Calibration Step: Semantic Level */
8  $\mathcal{S}_o^y = \emptyset$ ,  $tp_y = 0$  and  $fn_y = 0$  for  $\forall y \in \mathcal{Y} \setminus \{1\}$ ;
9 for  $(\mathbf{X}_i, \mathbf{Y}_i) \in \mathcal{D}_{cali}$  do
10  | if  $\exists y \in \mathcal{Y}_r$ ,  $s_{kl}(\mathbf{X}, y) \leq q_o^y$  then
11  |   | add  $1 - f(\mathbf{X}_i)_y$  into  $\mathcal{S}_o^y$  and  $tp_y = tp_y + 1$  for  $y = \mathbf{Y}_i \in \mathcal{Y} \setminus \{1\}$ ;
12  | else
13  |   |  $fn_y = fn_y + 1$  for  $y = \mathbf{Y}_i \in \mathcal{Y} \setminus \{1\}$ ;
14  | end
15 end
16 for  $y \in \mathcal{Y} \setminus \{1\}$  do
17  |  $\alpha_o^y = 1 - \frac{tp_y}{tp_y + fn_y}$  if  $y \notin \mathcal{Y}_r$ 
18  |  $\alpha_s^y = 1 - \frac{1-\alpha^y}{1-\alpha_o^y}$ ;  $q_s^y = \text{Quantile}(\frac{\lceil (N_{yo}+1)(1-\alpha_s^y) \rceil}{N_{yo}}, \mathcal{S}_o^y)$  where  $N_{yo}^y = |\mathcal{S}_o^y|$ 
19 end
20 /* Test Step */
21 for  $\mathbf{X}_i \in \mathcal{D}_{test}$  do
22  | if  $\exists y \in \mathcal{Y}_r$ ,  $s_{kl}(\mathbf{X}, y) \leq q_o^y$  then
23  |   |  $\mathcal{C}(\mathbf{X}_i) = \{y : 1 - f(\mathbf{X}_i)_y \leq q_s^y\}$ 
24  | else
25  |   |  $\mathcal{C}(\mathbf{X}_i) = \emptyset$  which means it is empty class.
26  | end
27 end

```

Current CP does not consider the hierarchical structure of classification, such as the geometry completion and semantic segmentation in SSC models. Here we propose a novel hierarchical conformal prediction (HCP) to address these challenges, which is shown in Algo.1.

Geometric Level. On the geometric level, it is important and safety-critical to guarantee the occupied recall of some sensitive classes, such as the person. Hence, we define the occupied coverage for the specific safety-critical class y (e.g., person, bike classes for AVs) as:

$$\mathbb{P}(o = T | \mathbf{Y}_{test} = y) \geq 1 - \alpha_o^y, \quad (5)$$

the probability of the voxels with label y are predicted as occupied is guaranteed to be no smaller than $1 - \alpha_o^y$. The empty class is $y = 1$ and the occupied classes are $y \in \{2, \dots, M\}$. To achieve the above guarantee under the high class-imbalanced dataset, we propose a novel score function based on the KL divergence. Here we define the ground-truth distribution for occupancy as $\mathbf{O} = \{\varepsilon, 1, \dots, 1\}^M$, where ε is the minimum value for the empty class. With the output probability $f(\mathbf{X}) = \{p_1, p_2, \dots, p_M\}$ by the model f , we define the KL-based score function for $y \in \mathcal{Y}_r$, different from $s(\mathbf{X}, y) = 1 - f(\mathbf{X})_y$:

$$s_{kl}(\mathbf{X}, y) = D_{kl}(f(\mathbf{X}) || \mathbf{O}) = p_1 \log\left(\frac{p_1}{\varepsilon}\right) + \sum_{i=2}^M p_i \log(p_i), \text{ for } \mathbf{X} \in \Upsilon^y, \quad (6)$$

where Υ^y is the subset of the calibration dataset with $\mathbf{Y} = y$, and \mathcal{Y}_r is the considered rare class set. The quantile q_o^y for class y is the $\frac{\lceil (N_y+1)(1-\alpha_o^y) \rceil}{N_y}$ quantile of the score $s_{kl}(\mathbf{X}, y)$ on Υ^y where $N_y = |\Upsilon^y|$. Then we predict the voxel \mathbf{X}_{test} as occupied if $\exists y \in \mathcal{Y}_r, s_{kl}(\mathbf{X}_{test}, y) \leq q_o^y$.

Semantic Level. On the semantic level, we need to achieve the same class-balanced coverage as Eq. 4, under the geometric level coverage guarantee. For all voxels which are predicted as occupied in the previous step, we generate the prediction set $\mathcal{C}(\mathbf{X}_{test}) \subset \{2, \dots, M\}$ to satisfy the guarantee:

$$\mathbb{P}(\mathbf{Y} \in \mathcal{C}(\mathbf{X}_{test}) | \mathbf{Y} = y, o = T) \geq 1 - \alpha_s^y \quad (7)$$

The score function here is $s(\mathbf{X}, y) = 1 - f(\mathbf{X})_y$. We compute the quantile q_s^y for class y as the $\frac{\lceil (N_{y_o}+1)(1-\alpha_s^y) \rceil}{N_{y_o}}$ quantile of the score on Υ_o^y , where Υ_o^y is the subset of the calibration dataset that has label y and are predicted as occupied on the geometric level of our HCP, $N_{y_o} = |\Upsilon_o^y|$.

The prediction set is generated as:

$$\mathcal{C}(\mathbf{X}_{test}) = \{y : s_{kl}(\mathbf{X}, y) \leq q_o^y \wedge s(\mathbf{X}, y) \leq q_s^y\} \quad (8)$$

Proposition 1. In Alg.1, for a desired α^y value, we select α_o^y and α_s^y as $1 - \alpha^y = (1 - \alpha_o^y)(1 - \alpha_s^y)$, then the prediction set generated as Eq. 8 satisfies $\mathbb{P}(\mathbf{Y}_{test} \in \mathcal{C}(\mathbf{X}_{test}) | \mathbf{Y}_{test} = y) \geq 1 - \alpha^y$. The proof is in Appendix 5.2.

4 Experiments

SSC Model. We assess the effectiveness of our approach through comprehensive experiments on one CSSC model VoxFormer (Li et al. [2023b]). It features a two-stage process: generating sparse visible voxel queries from depth estimation, followed by densification into dense 3D voxels. It outperforms other CSSC methods in accuracy and efficiency, achieving significant improvements in geometry and semantics with reduced GPU memory usage. **Dataset.** The datasets we used are SemanticKITTI (Behley et al. [2019], with 20 classes) and SSCBench-KITTI-360 (Li et al. [2023a], with 19 classes). More details on experiments are shown in Appendix 5.

4.1 Uncertainty Propagation Performance

Table 1: Performance evaluation of our Depth-UP on VoxFormer.

Dataset	Method	IoU \uparrow	Precision \uparrow	Recall \uparrow	mIoU \uparrow	mIoU \uparrow		
						bicycle	motorcycle	person
SemanticKITTI	Base	44.02	62.32	59.99	12.35	0.59	0.51	1.78
	Our	45.85	63.1	62.64	13.36	0.12	3.57	2.24
KITTI360	Base	38.76	57.67	54.18	11.91	1.16	0.89	1.63
	Our	43.25	65.81	55.78	13.65	1.96	1.58	3.13

Metric. For SSC performance, we employ the intersection over union (IoU) to evaluate the geometric completion, regardless of the allocated semantic labels. This is very crucial for obstacle avoidance for

autonomous vehicles. We use the mean IoU (mIoU) of all semantic classes to assess the performance of semantic segmentation of SSC. Since there is a strong negative correlation between IoU and mIoU (Li et al. [2023b]), the model should achieve excellent performance in both geometric completion and semantic segmentation.

The experimental results of our Depth-UP framework on VoxFormer using the SemanticKITTI and KITTI360 datasets are presented in Table 1. These results demonstrate that Depth-UP effectively leverages quantified uncertainty from the depth model to enhance CSSC model performance, achieving up to a 4.49 (11.58%) improvement in IoU and up to a 1.74 (14.61%) improvement in mIoU, while also significantly improving both precision and recall in the geometry completion aspect of CSSC. When accessing the performance of CSSC models, even slight improvements in IoU and mIoU mean good progress, as reported by Zhang et al. [2023], Huang et al. [2023]. In Table 1, the mIoU results of some rare classes are shown in the right part. In most cases, our Depth-UP can improve mIoU of these classes for utilizing the depth uncertainty.

Figure 3 presents visualizations of the SSC model with and without our Depth-UP on SemanticKITTI. In this figure, we can also see that our Depth-UP can help the SSC model to predict rare classes, such as persons and bicyclists, as highlighted with the orange dashed boxes. Especially for the third row, our Depth-UP predicts the person crossing the road in the corner, while the baseline ignores him. Our Depth-UP can significantly reduce the risk of hurting humans for AVs and improve safety.

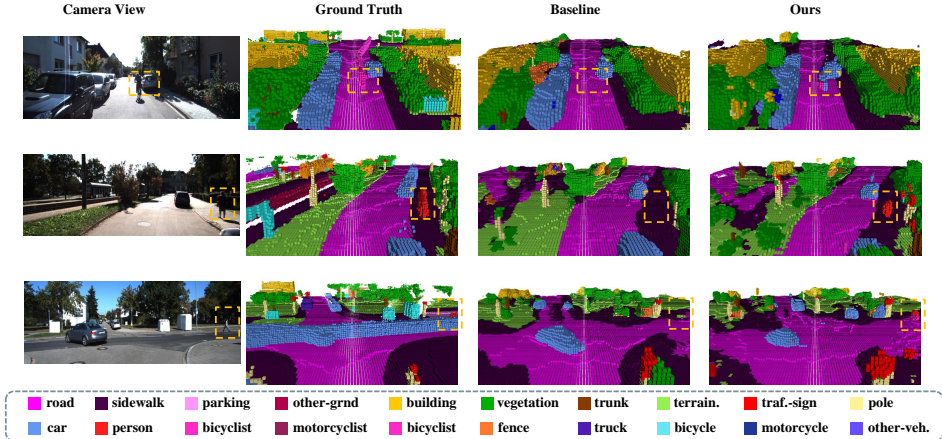


Figure 3: Qualitative results of the baseline SSC model and that with our Depth-UP method.

4.2 Uncertainty Quantification Performance

We evaluate our HCP on the geometrical level and the uncertainty quantification. In the experiments here, since we do not have test part of SemanticKITTI, we randomly split the original validation part of SemanticKITTI into the calibration dataset (take up 30%) and the test dataset (take up 70%). For KITTI360, we use the validation part as the calibration dataset and the test part as the test dataset.

Geometrical Level. For the geometry level, the target of methods is to achieve the best trade-off between IoU performance and the occupied recall of rare classes. To show the effectiveness of our novel KL-based score function on the geometric level, we compare it with two common score functions (Angelopoulos and Bates [2021]): class score $(1 - f(\mathbf{X})_y)$ and occupied score $(1 - \sum_{y=2}^M f(\mathbf{X})_y)$. Figure 4 shows the IoU results across different occupied recall of the considered rare class (person, $1 - \alpha_0^{person}$) for different SSC models and datasets. The red dotted line shows the IoU of the SSC model without UQ methods. We can see that our KL-based score function always achieves the best geometry performance for the same occupied recall, compared with two baselines. The two base score functions perform so badly because they cannot handle the high-level class imbalance in SSC. To achieve the optimal balance between IoU and occupied recall, we can adjust the occupied recall metric. For instance, in the second subfigure, the SSC model without HCP shows an IoU of 45.85 and an occupied recall for the person class of 20.69. By setting the occupied recall to 21.75, the IoU performance improves to 45.94. And, increasing the occupied recall beyond 30 (45.0% improvement) results in a decrease in IoU to 44.38 (3.4% reduction). This demonstrates that our HCP method can substantially boost the occupied recall of rare classes with only a minor reduction in IoU.

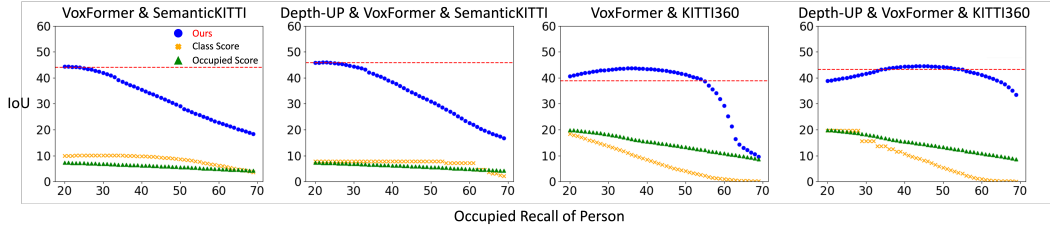


Figure 4: Compare our KL-based score function with the class score function and the occupied score function. SSC’s IoU performance across occupied recall of considered rare class (person). The red dotted line shows the IoU of the SSC model without UQ methods. Our KL-based score function always achieves the highest IoU for the same occupied recall, compared with the other two baselines.

Uncertainty Quantification. Metric: To measure the quantified uncertainty for different conformal prediction methods, we usually use the average class coverage gap (CovGap) and average set size (AvgSize) of the prediction sets (Ding et al. [2024]). For a given class $y \in \mathcal{Y} \setminus \{1\}$ with the defined error rate α^y , the empirical class-conditional coverage of class y is $c_y = \frac{1}{|\mathcal{T}^y|} \sum_{i \in \mathcal{T}^y} \mathbb{I}\{\mathbf{Y}_i \in \mathcal{C}(\mathbf{X}_i)\}$. The CovGap is defined as $\frac{1}{|\mathcal{Y}| - 1} \sum_{y \in \mathcal{Y} \setminus \{1\}} |c_y - (1 - \alpha^y)|$. This measures how far the class-conditional coverage is from the desired coverage level of $1 - \alpha^y$. The AvgSize is defined as $\frac{1}{T} \sum_{i=1}^T |\mathcal{C}(\mathbf{X}_i)|$, where T is the number of samples in the test dataset and $\mathcal{C}(\mathbf{X}_i)$ does not contain the empty class. A good UQ method should achieve both small CovGap and AvgSize.

Table 2 compares our HCP method with standard conformal prediction (SCP) and class-conditional conformal prediction (CCCP), as introduced in Subsection 3.3.1, using the CovGap and AvgSize. Our results demonstrate that HCP consistently achieves robust empirical class-conditional coverage and produces smaller prediction sets. In contrast, the performance of SCP and CCCP varies across different SSC models. Specifically, for the SSC model combined with our Depth-UP on KITTI360, HCP reduces set sizes by 33% with a comparable coverage gap to CCCP. Compared to SCP, HCP reduces set sizes by 85% and coverage gap by 91%. As noted in Subsection 3.3.1, SCP consistently fails to provide conditional coverage. Both SCP and CCCP tend to generate nonempty $\mathcal{C}(\mathbf{X})$ for most voxels, potentially obstructing autonomous vehicles, as illustrated in Figure 1.c.ii. In contrast, HCP selectively targets occupied voxels, generating nonempty $\mathcal{C}(\mathbf{X})$ only for these, thereby minimizing prediction set sizes while maintaining reliable class-conditional coverage.

Table 2: Compare our HCP with the standard conformal prediction (SCP) and class-conditional conformal prediction (CCCP) on CovGap and AvgSize.

Dataset	SemanticKITTI						KITTI360					
	Base			Our Depth-UP			Base			Our Depth-UP		
UQ Method	SCP	CCCP	Ours	SCP	CCCP	Ours	SCP	CCCP	Ours	SCP	CCCP	Ours
CovGap ↓	0.52	0.22	0.10	0.21	0.03	0.04	0.39	0.06	0.06	0.53	0.04	0.05
AvgSize ↓	1.02	6.43	1.39	1.52	1.59	1.02	4.66	0.62	0.42	5.22	0.25	0.17

4.3 Ablation Study

Table 3: Ablation study on our Depth-UP framework with VoxFormer and SemanticKITTI.

PGC	PSS	IoU ↑	Precision ↑	Recall ↑	mIoU ↑	FPS ↑
		44.02	62.32	59.99	12.35	8.85
✓		44.91	63.76	60.30	12.58	7.14
	✓	44.40	62.69	60.35	12.77	8.76
✓	✓	45.85	63.10	62.64	13.36	7.08

We conducted an ablation study to assess the contributions of each technique proposed in our Depth-UP, as detailed in Table 3. The best results are shown in bold. The results indicate that Propagation on Geometry Completion (PGC) significantly enhances IoU, precision, and recall, which are key metrics for geometry. Additionally, Propagation on Semantic Segmentation (PSS) markedly improves mIoU, a crucial metric for semantic accuracy. Notably, the combined application of both techniques yields performance improvements that surpass the sum of their individual contributions.

Limitation. Regarding frames per second (FPS), our Depth-UP results in a 20% decrease. However, this reduction does not significantly impact the overall efficiency of SSC models. It is important to note that we have not implemented any specific code optimization strategies to enhance runtime. Consequently, the computational overhead introduced by our framework remains acceptable.

5 Conclusion

This paper introduces a novel approach to enhancing camera-based 3D Semantic Scene Completion (SSC) for AVs by incorporating uncertainty inherent in models. Our proposed framework, α -SSC, integrates the uncertainty propagation from depth models (Depth-UP) to improve SSC performance in both geometry completion and semantic segmentation. A novel hierarchical conformal prediction (HCP) method is designed to quantify SSC uncertainty effectively under high-level class imbalance. Our extensive experiments demonstrate the effectiveness of our α -SSC. The Depth-UP significantly improves prediction accuracy, achieving up to 11.58% increase in IoU and up to 14.61% increase in mIoU. The HCP further enhances performance by achieving robust class-conditional coverage and reducing prediction set sizes. Compared to baselines, it reduces up to 85% set sizes and up to 91% coverage gap. These results highlight the significant improvements in both accuracy and uncertainty quantification offered by our approach, especially for rare safety-critical classes, such as persons and bicyclists, thereby reducing potential risks for AVs. In the future, we will extend HCP to be applicable to other highly imbalanced classification tasks.

References

- Anastasios N Angelopoulos and Stephen Bates. A gentle introduction to conformal prediction and distribution-free uncertainty quantification. *arXiv preprint arXiv:2107.07511*, 2021.
- George B Arfken, Hans J Weber, and Frank E Harris. *Mathematical methods for physicists: a comprehensive guide*. Academic press, 2011.
- Vijay Badrinarayanan, Alex Kendall, and Roberto Cipolla. Segnet: A deep convolutional encoder-decoder architecture for image segmentation. *IEEE transactions on pattern analysis and machine intelligence*, 39(12):2481–2495, 2017.
- Jens Behley, Martin Garbade, Andres Milioto, Jan Quenzel, Sven Behnke, Cyrill Stachniss, and Jurgen Gall. Semantickitti: A dataset for semantic scene understanding of lidar sequences. In *Proceedings of the IEEE/CVF international conference on computer vision*, pages 9297–9307, 2019.
- Shariq Farooq Bhat, Ibraheem Alhashim, and Peter Wonka. Adabins: Depth estimation using adaptive bins. In *Proceedings of the IEEE/CVF conference on computer vision and pattern recognition*, pages 4009–4018, 2021.
- Mateusz Buda, Atsuto Maki, and Maciej A Mazurowski. A systematic study of the class imbalance problem in convolutional neural networks. *Neural networks*, 106:249–259, 2018.
- Anh-Quan Cao and Raoul De Charette. Monoscene: Monocular 3d semantic scene completion. In *Proceedings of the IEEE/CVF Conference on Computer Vision and Pattern Recognition*, pages 3991–4001, 2022.
- Robin Chan, Matthias Rottmann, Fabian Hüger, Peter Schlicht, and Hanno Gottschalk. Application of decision rules for handling class imbalance in semantic segmentation. *arXiv preprint arXiv:1901.08394*, 2019.
- Bike Chen, Chen Gong, and Jian Yang. Importance-aware semantic segmentation for autonomous vehicles. *IEEE Transactions on Intelligent Transportation Systems*, 20(1):137–148, 2018.
- Ran Cheng, Christopher Agia, Yuan Ren, Xinhai Li, and Liu Bingbing. S3cnet: A sparse semantic scene completion network for lidar point clouds. In *Conference on Robot Learning*, pages 2148–2161. PMLR, 2021.
- Tiffany Ding, Anastasios Angelopoulos, Stephen Bates, Michael Jordan, and Ryan J Tibshirani. Class-conditional conformal prediction with many classes. *Advances in Neural Information Processing Systems*, 36, 2024.
- David Eigen and Rob Fergus. Predicting depth, surface normals and semantic labels with a common multi-scale convolutional architecture. In *Proceedings of the IEEE international conference on computer vision*, pages 2650–2658, 2015.

- Di Feng, Ali Harakeh, Steven L Waslander, and Klaus Dietmayer. A review and comparative study on probabilistic object detection in autonomous driving. *IEEE Transactions on Intelligent Transportation Systems*, 23(8):9961–9980, 2021.
- Andreas Geiger, Philip Lenz, and Raquel Urtasun. Are we ready for autonomous driving? the kitti vision benchmark suite. In *2012 IEEE conference on computer vision and pattern recognition*, pages 3354–3361. IEEE, 2012.
- Kaiming He, Xiangyu Zhang, Shaoqing Ren, and Jian Sun. Deep residual learning for image recognition. In *Proceedings of the IEEE conference on computer vision and pattern recognition*, pages 770–778, 2016.
- Sihong He, Songyang Han, Sanbao Su, Shuo Han, Shaofeng Zou, and Fei Miao. Robust multi-agent reinforcement learning with state uncertainty. *arXiv preprint arXiv:2307.16212*, 2023.
- Yihan Hu, Jiazhi Yang, Li Chen, Keyu Li, Chonghao Sima, Xizhou Zhu, Siqi Chai, Senyao Du, Tianwei Lin, Wenhai Wang, et al. Planning-oriented autonomous driving. In *Proceedings of the IEEE/CVF Conference on Computer Vision and Pattern Recognition*, pages 17853–17862, 2023.
- Yuanhui Huang, Wenzhao Zheng, Yunpeng Zhang, Jie Zhou, and Jiwen Lu. Tri-perspective view for vision-based 3d semantic occupancy prediction. In *Proceedings of the IEEE/CVF conference on computer vision and pattern recognition*, pages 9223–9232, 2023.
- Ashkan M Jasour and Brian C Williams. Risk contours map for risk bounded motion planning under perception uncertainties. In *Robotics: Science and Systems*, pages 22–26, 2019.
- Balaji Lakshminarayanan, Alexander Pritzel, and Charles Blundell. Simple and scalable predictive uncertainty estimation using deep ensembles. *Advances in neural information processing systems*, 30, 2017.
- Yiming Li, Sihang Li, Xinhao Liu, Moonjun Gong, Kenan Li, Nuo Chen, Zijun Wang, Zhiheng Li, Tao Jiang, Fisher Yu, et al. Sscbench: A large-scale 3d semantic scene completion benchmark for autonomous driving. *arXiv preprint arXiv:2306.09001*, 2023a.
- Yiming Li, Zhiding Yu, Christopher Choy, Chaowei Xiao, Jose M Alvarez, Sanja Fidler, Chen Feng, and Anima Anandkumar. Voxformer: Sparse voxel transformer for camera-based 3d semantic scene completion. In *Proceedings of the IEEE/CVF conference on computer vision and pattern recognition*, pages 9087–9098, 2023b.
- Yiqing Liang, Boyuan Chen, and Shuran Song. Sscnav: Confidence-aware semantic scene completion for visual navigation. In *2021 IEEE International Conference on Robotics and Automation (ICRA)*, pages 13194–13200. IEEE, 2021.
- Yiyi Liao, Jun Xie, and Andreas Geiger. Kitti-360: A novel dataset and benchmarks for urban scene understanding in 2d and 3d. *IEEE Transactions on Pattern Analysis and Machine Intelligence*, 45(3):3292–3310, 2022.
- Tsung-Yi Lin, Priya Goyal, Ross Girshick, Kaiming He, and Piotr Dollár. Focal loss for dense object detection. In *Proceedings of the IEEE international conference on computer vision*, pages 2980–2988, 2017.
- Yan Lu, Xinzhu Ma, Lei Yang, Tianzhu Zhang, Yating Liu, Qi Chu, Junjie Yan, and Wanli Ouyang. Geometry uncertainty projection network for monocular 3d object detection. In *Proceedings of the IEEE/CVF International Conference on Computer Vision*, pages 3111–3121, 2021.
- Fadel M Megahed, Ying-Ju Chen, Aly Megahed, Yuya Ong, Naomi Altman, and Martin Krzywinski. The class imbalance problem. *Nat Methods*, 18(11):1270–7, 2021.
- Gregory P Meyer and Niranjan Thakurdesai. Learning an uncertainty-aware object detector for autonomous driving. In *2020 IEEE/RSJ International Conference on Intelligent Robots and Systems (IROS)*, pages 10521–10527. IEEE, 2020.
- Dimity Miller, Lachlan Nicholson, Feras Dayoub, and Niko Sünderhauf. Dropout sampling for robust object detection in open-set conditions. In *2018 IEEE International Conference on Robotics and Automation (ICRA)*, pages 3243–3249. IEEE, 2018.

- Kevin P Murphy. *Machine learning: a probabilistic perspective*. MIT press, 2012.
- Matteo Poggi, Filippo Aleotti, Fabio Tosi, and Stefano Mattoccia. On the uncertainty of self-supervised monocular depth estimation. In *Proceedings of the IEEE/CVF Conference on Computer Vision and Pattern Recognition*, pages 3227–3237, 2020.
- Luis Roldao, Raoul de Charette, and Anne Verroust-Blondet. Lmscnet: Lightweight multiscale 3d semantic completion. In *2020 International Conference on 3D Vision (3DV)*, pages 111–119. IEEE, 2020.
- Faranak Shamsafar, Samuel Woerz, Rafia Rahim, and Andreas Zell. Mobilestereonet: Towards lightweight deep networks for stereo matching. In *Proceedings of the IEEE/CVF winter conference on applications of computer vision*, pages 2417–2426, 2022.
- Shuran Song, Fisher Yu, Andy Zeng, Angel X Chang, Manolis Savva, and Thomas Funkhouser. Semantic scene completion from a single depth image. In *Proceedings of the IEEE conference on computer vision and pattern recognition*, pages 1746–1754, 2017.
- Sanbao Su, Yiming Li, Sihong He, Songyang Han, Chen Feng, Caiwen Ding, and Fei Miao. Uncertainty quantification of collaborative detection for self-driving. In *2023 IEEE International Conference on Robotics and Automation (ICRA)*, pages 5588–5594. IEEE, 2023.
- Junjiao Tian, Yen-Cheng Liu, Nathaniel Glaser, Yen-Chang Hsu, and Zsolt Kira. Posterior recalibration for imbalanced datasets. *Advances in neural information processing systems*, 33: 8101–8113, 2020.
- Xiaoyu Tian, Tao Jiang, Longfei Yun, Yucheng Mao, Huitong Yang, Yue Wang, Yilun Wang, and Hang Zhao. Occ3d: A large-scale 3d occupancy prediction benchmark for autonomous driving. *Advances in Neural Information Processing Systems*, 36, 2024.
- Jason Van Hulse, Taghi M Khoshgoftaar, and Amri Napolitano. Experimental perspectives on learning from imbalanced data. In *Proceedings of the 24th international conference on Machine learning*, pages 935–942, 2007.
- Lele Wang and Yingping Huang. A survey of 3d point cloud and deep learning-based approaches for scene understanding in autonomous driving. *IEEE Intelligent Transportation Systems Magazine*, 14(6):135–154, 2021.
- Yuqi Wang, Yuntao Chen, and Zhaoxiang Zhang. Frustumformer: Adaptive instance-aware resampling for multi-view 3d detection. In *Proceedings of the IEEE/CVF Conference on Computer Vision and Pattern Recognition*, pages 5096–5105, 2023.
- Wenda Xu, Jia Pan, Junqing Wei, and John M Dolan. Motion planning under uncertainty for on-road autonomous driving. In *2014 IEEE International Conference on Robotics and Automation (ICRA)*, pages 2507–2512. IEEE, 2014.
- Xu Yan, Jiantao Gao, Jie Li, Ruimao Zhang, Zhen Li, Rui Huang, and Shuguang Cui. Sparse single sweep lidar point cloud segmentation via learning contextual shape priors from scene completion. In *Proceedings of the AAAI Conference on Artificial Intelligence*, volume 35, pages 3101–3109, 2021.
- Yunpeng Zhang, Zheng Zhu, and Dalong Du. Occformer: Dual-path transformer for vision-based 3d semantic occupancy prediction. In *Proceedings of the IEEE/CVF International Conference on Computer Vision*, pages 9433–9443, 2023.

Appendix

5.1 More Related Work

Class Imbalance. In real-world applications like robotics and autonomous vehicles (AVs), datasets often face the challenge of class imbalance (Chen et al. [2018]). Underrepresented classes, typically encompassing high safety-critical entities such as people, are significantly outnumbered by lower safety-critical classes like trees and buildings. Various strategies have been proposed to tackle class imbalance. Data-level methods involve random under-sampling of majority classes and over-sampling of minority classes during training (Van Hulse et al. [2007]). However, they struggle to address the pronounced class imbalance encountered in SSC (Megahed et al. [2021]), as shown in Section 1. Algorithm-level methods employ cost-sensitive losses to adjust the training process for different tasks, such as depth estimation (Eigen and Fergus [2015]) and 2D segmentation (Badrinarayanan et al. [2017]). While algorithm-level methods have been widely implemented in current SSC models (Voxformer (Li et al. [2023b]) utilizes Focal Loss Lin et al. [2017] as the loss function), they still fall short in accurately predicting minority classes. In contrast, classifier-level methods adjust output class probabilities during the testing phase through posterior calibration (Buda et al. [2018], Tian et al. [2020]). In this paper, we propose a hierarchical conformal prediction method falling within this category, aimed at enhancing the recall of underrepresented safety-critical classes in the SSC task.

5.2 Proof of Proposition 1

Proposition 1. In Alg.1, for a desired α^y value, we select α_o^y and α_s^y as $1 - \alpha^y = (1 - \alpha_s^y)(1 - \alpha_o^y)$, then the prediction set generated as Eq. 8 satisfies that $\mathbb{P}(\mathbf{Y}_{test} \in \mathcal{C}(\mathbf{X}_{test}) | \mathbf{Y}_{test} = y) \geq 1 - \alpha^y$.

Proof.

$$\begin{aligned} \mathbb{P}(\mathbf{Y}_{test} \in \mathcal{C}(\mathbf{X}_{test}) | \mathbf{Y}_{test} = y) &= \sum_o \mathbb{P}(\mathbf{Y} \in \mathcal{C}(\mathbf{X}_{test}) | \mathbf{Y}_{test} = y, o) \mathbb{P}(o | \mathbf{Y}_{test} = y) \\ &= \mathbb{P}(\mathbf{Y}_{test} \in \mathcal{C}(\mathbf{X}_{test}) | \mathbf{Y}_{test} = y, o = T) \mathbb{P}(o = T | \mathbf{Y}_{test} = y) \\ &\quad + \mathbb{P}(\mathbf{Y}_{test} \in \mathcal{C}(\mathbf{X}_{test}) | \mathbf{Y}_{test} = y, o = F) \mathbb{P}(o = F | \mathbf{Y}_{test} = y) \\ &= \mathbb{P}(\mathbf{Y}_{test} \in \mathcal{C}(\mathbf{X}_{test}) | \mathbf{Y}_{test} = y, o = T) \mathbb{P}(o = T | \mathbf{Y}_{test} = y) \geq (1 - \alpha_s^y)(1 - \alpha_o^y) \\ &\Rightarrow \mathbb{P}(\mathbf{Y}_{test} \in \mathcal{C}(\mathbf{X}_{test}) | \mathbf{Y}_{test} = y) \geq 1 - \alpha^y, \text{ when } 1 - \alpha^y = (1 - \alpha_s^y)(1 - \alpha_o^y) \end{aligned}$$

□

5.3 Introduction on Datasets

During the experiments, we use two datasets: SemanticKITTI (Behley et al. [2019]) and SSCBench-KITTI-360 (Li et al. [2023a]). SemanticKITTI provides dense semantic annotations for each LiDAR sweep composed of 22 outdoor driving scenarios based on the KITTI Odometry Benchmark (Geiger et al. [2012]). Regarding the sparse input to an SSC model, it can be either a single voxelized LiDAR sweep or an RGB image. The voxel grids are labeled with 20 classes (19 semantics and 1 empty), with the size of $0.2\text{m} \times 0.2\text{m} \times 0.2\text{m}$. We only used the train and validation parts of SemanticKITTI as the annotations of the test part are not available. SSCBench-KITTI-360 provides dense semantic annotations for each image based on KITTI-360 (Liao et al. [2022]), which is called KITTI360 for simplification. The voxel grids are labeled with 19 classes (18 semantics and 1 empty), with the size of $0.2\text{m} \times 0.2\text{m} \times 0.2\text{m}$. Both SemanticKITTI and SSCBench-KITTI-360 are interested in a volume of 51.2m ahead of the car, 25.6m to left and right side, and 6.4m in height.

5.4 Experimental Setting

We utilized two different servers to conduct experiments on the Semantic KITTI and KITTI360 datasets. For the Semantic KITTI dataset, we employed a system equipped with four NVIDIA Quadro RTX 8000 GPUs, each providing 48GB of VRAM. The system was configured with 128GB of system RAM. The training process required approximately 30 minutes per epoch, culminating in a total training duration of around 16 hours for 30 epochs. The software environment included the Linux operating system (version 18.04), Python 3.8.19, CUDA 11.1, PyTorch 1.9.1+cu111, and CuDNN 8.0.5.

Table 4: **Separate results on SemanticKITTI and KITTI360.** We evaluate our Depth-UP models on two datasets. The default evaluation range is $51.2 \times 51.2 \times 6.4\text{m}^3$. Due to the label differences amongst the two subsets, missing labels are replaced with "-". The top three performances on each dataset are marked by **red**, **green**, and **blue** respectively.

Dataset	Method	Input	IoU	mIoU	car	bicycle	motorcycle	truck	other-veh.	person	road	parking	sidewalk	other-grnd	building	fence	vegetation	terrain	pole	traf.-sign	bicyclist	trunk
SemanticKITTI	LMSCNet	L	38.36	9.94	23.62	0.00	0.00	1.69	0.00	0.00	54.9	9.89	25.43	0.00	14.55	3.27	20.19	32.3	2.04	0.00	0.00	1.06
	SSCNet	L	40.93	10.27	22.32	0.00	0.00	4.69	2.43	0.00	51.28	9.07	22.38	0.02	15.2	3.57	22.24	31.21	4.83	1.49	0.01	4.33
	MonoScene	C	36.80	11.30	23.29	0.28	0.59	9.29	2.63	2.00	55.89	14.75	26.50	1.63	13.55	6.60	17.98	29.84	3.91	2.43	1.07	2.44
	Voxformer	C	44.02	12.35	25.79	0.59	0.51	5.63	3.77	1.78	54.76	15.50	26.35	0.70	17.65	7.64	24.39	29.96	7.11	4.18	3.32	5.08
	TPVFormer	C	35.61	11.36	23.81	0.36	0.05	8.08	4.35	0.51	56.50	20.60	25.87	0.85	13.88	5.94	16.92	30.38	3.14	1.52	0.89	2.26
	OccFormer	C	36.50	13.46	25.09	0.81	1.19	25.53	8.52	2.78	58.85	19.61	26.88	0.31	14.40	5.61	19.63	32.62	4.26	2.86	2.82	3.93
	Depth-UP (ours)	C	45.85	13.36	28.51	0.12	3.57	12.01	4.23	2.24	55.72	14.38	26.20	0.10	20.58	7.70	26.24	30.26	8.03	5.81	1.18	7.03
KITTI-360	LMSCNet	L	47.53	13.65	20.91	0	0	0.26	0	0	62.95	13.51	33.51	0.2	43.67	0.33	40.01	26.80	0	0	-	-
	SSCNet	L	53.58	16.95	31.95	0	0.17	10.29	0.58	0.07	65.7	17.33	41.24	3.22	44.41	6.77	43.72	28.87	0.78	0.75	-	-
	MonoScene	C	37.87	12.31	19.34	0.43	0.58	8.02	2.03	0.86	48.35	11.38	28.13	3.22	32.89	3.53	26.15	16.75	6.92	5.67	-	-
	Voxformer v1	C	38.76	11.91	17.84	1.16	0.89	4.56	2.06	1.63	47.01	9.67	27.21	2.89	31.18	4.97	28.99	14.69	6.51	6.92	-	-
	TPVFormer	C	40.22	13.64	21.56	1.09	1.37	8.06	2.57	2.38	52.99	11.99	31.07	3.78	34.83	4.80	30.08	17.51	7.46	5.86	-	-
	OccFormer	C	40.27	13.81	22.58	0.66	0.26	9.89	3.82	2.77	54.3	13.44	31.53	3.55	36.42	4.80	31.00	19.51	7.77	8.51	-	-
	Depth-UP (ours)	C	43.25	13.55	22.32	1.96	1.58	9.43	2.27	3.13	53.50	11.86	31.63	3.20	34.49	6.11	32.01	18.78	11.46	13.65	-	-

For the KITTI360 dataset, we used a different system equipped with eight NVIDIA GeForce RTX 4090 GPUs, each providing 24GB of VRAM, with 720GB of system RAM. The training process required approximately 15 minutes per epoch, culminating in a total training duration of around 8 hours for 30 epochs. The software environment comprised the Linux operating system (version 18.04), Python 3.8.16, CUDA 11.1, PyTorch 1.9.1+cu111, and CuDNN 8.0.5. These settings ensure the reproducibility of our experiments on similar hardware configurations.

In our training, we used the AdamW optimizer with a learning rate of $2e-4$ and a weight decay of 0.01. The learning rate schedule followed a Cosine Annealing policy with a linear warmup for the first 500 iterations, starting at a warmup ratio of $\frac{1}{3}$. The minimum learning rate ratio was set to $1e-3$. We applied gradient clipping with a maximum norm of 35 to stabilize the training.

The user-defined target error rate α_y for each class y is decided according to the prediction error rate of the original model. For example, for the person class, the original model has 90% prediction error rate, and the user-defined target error rate α_{person} of person is decided as $90\% * 0.8 = 72\%$.

5.5 More Results on Depth-UP

Table 4 presents a comparative analysis of our Depth-UP models against various SSC models, providing detailed mIoU results for different classes. Our Depth-UP demonstrates superior performance in geometry completion, outperforming all other camera-based SSC (CSSC) models and even surpassing LiDAR-based SSC models on the SemanticKITTI dataset. This improvement is attributed to the significant influence of depth estimation on geometry performance and the effective utilization of inherent uncertainty in depth. In terms of semantic segmentation, our Depth-UP achieves performance comparable to state-of-the-art CSSC methods. Notably, on the KITTI360 dataset, our Depth-UP achieves the highest mIoU for bicycle, motorcycle, and person classes, which are crucial for safety.

Figure 5 provides additional visualizations of the SSC model’s performance with and without our Depth-UP on the SemanticKITTI dataset. These visualizations demonstrate that our Depth-UP enhances the model’s ability to predict rare classes, such as persons and bicyclists, which are highlighted with orange dashed boxes. Notably, in the fourth row, our Depth-UP successfully predicts the presence of a person far from the camera, whereas the baseline model fails to do so. This indicates that Depth-UP improves object prediction in distant regions. By enhancing the detection of such critical objects, our Depth-UP significantly reduces the risk of accidents, thereby improving the safety of autonomous vehicles.

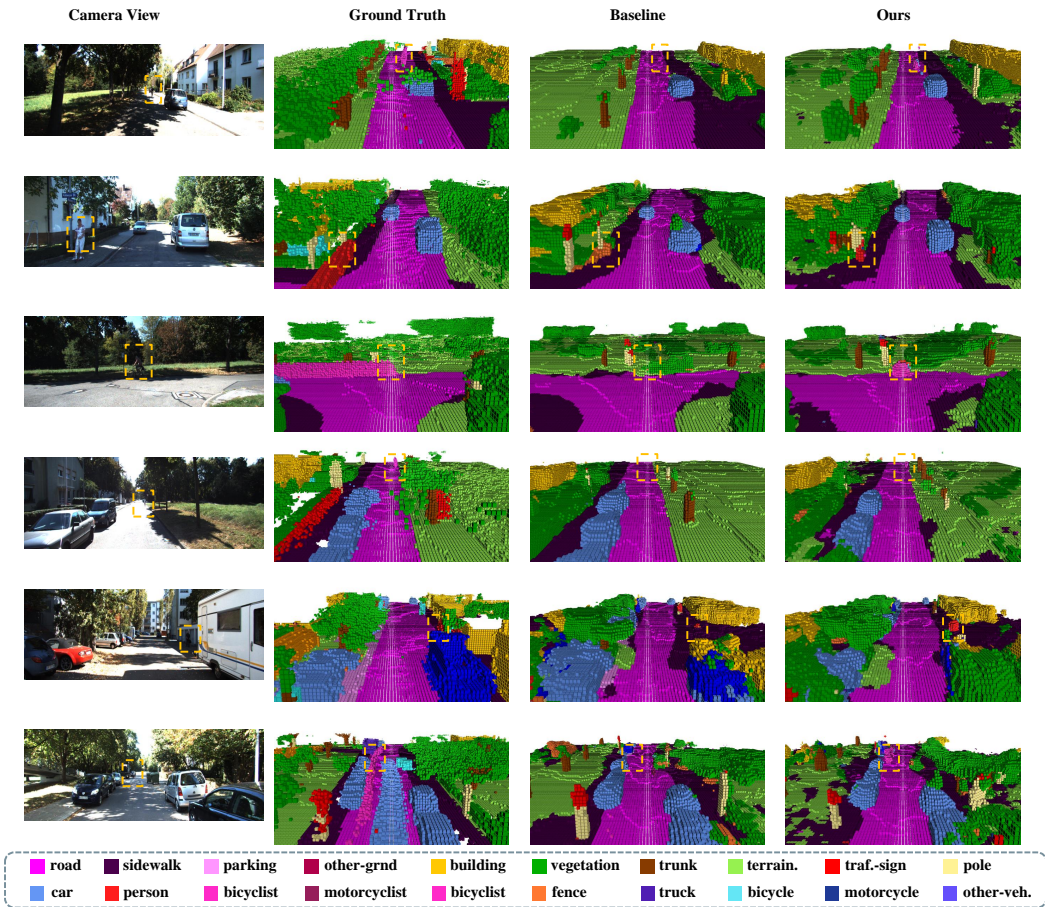


Figure 5: Qualitative results of the baseline SSC model and that with our Depth-UP method.

5.6 More Results on HCP

Table 5 and Table 6 provide a detailed analysis of the coverage gaps for each non-empty class, comparing our HCP method with baseline methods on the SemanticKITTI and KITTI360 datasets. These tables extend the results presented in Table 2. Our HCP method consistently achieves the smallest coverage gaps across most classes, demonstrating its effectiveness in uncertainty quantification and coverage accuracy.

Table 5: SemanticKITTI Class CovGap Results

Class	Base			Our Depth-UP		
	SCP	CCCP	Ours	SCP	CCCP	Ours
car	0.03	0.01	0.04	0.02	0.01	0.01
bicycle	0.50	0.41	0.12	0.37	0.03	0.06
motorcycle	0.54	0.32	0.03	0.30	0.07	0.10
truck	0.06	0.08	0.01	0.01	0.06	0.03
other-vehicle	0.30	0.01	0.03	0.11	0.04	0.02
person	0.12	0.07	0.12	0.07	0.04	0.03
bicyclist	0.13	0.01	0.04	0.27	0.01	0.01
motorcyclist	0.78	0.19	0.03	0.52	0.20	0.18
road	0.20	0.01	0.01	0.08	0.01	0.00
parking	0.39	0.09	0.03	0.19	0.00	0.02
sidewalk	0.06	0.02	0.02	0.05	0.01	0.00
other-ground	0.59	0.27	0.13	0.61	0.03	0.03
building	0.25	0.01	0.01	0.27	0.02	0.02
fence	0.15	0.04	0.01	0.24	0.04	0.01
vegetation	0.36	0.02	0.08	0.40	0.02	0.02
trunk	0.35	0.50	0.04	0.19	0.00	0.03
terrain	0.02	0.00	0.02	0.07	0.00	0.00
pole	0.12	0.01	0.10	0.09	0.00	0.12
traffic-sign	0.00	0.00	0.02	0.08	0.02	0.02
CovGap	0.52	0.22	0.10	0.21	0.03	0.04
AvgSize	1.02	6.43	1.39	1.52	1.59	1.02

Table 6: KITTI360 Class CovGap Results

Class	Base			Our Depth-UP		
	SCP	CCCP	Our HCP	SCP	CCCP	Our HCP
car	0.52	0.07	0.07	0.54	0.06	0.06
bicycle	0.17	0.09	0.07	0.46	0.08	0.11
motorcycle	0.17	0.06	0.11	0.52	0.07	0.08
truck	0.43	0.08	0.06	0.62	0.02	0.00
other-vehicle	0.40	0.02	0.01	0.64	0.02	0.01
person	0.12	0.04	0.05	0.35	0.05	0.06
road	0.26	0.02	0.02	0.35	0.02	0.01
parking	0.63	0.08	0.06	0.66	0.07	0.04
sidewalk	0.35	0.09	0.09	0.50	0.05	0.07
other-ground	0.60	0.01	0.07	0.72	0.04	0.04
building	0.57	0.04	0.04	0.67	0.02	0.01
fence	0.55	0.01	0.03	0.60	0.01	0.00
vegetation	0.57	0.04	0.04	0.75	0.02	0.02
terrain	0.82	0.14	0.14	0.84	0.11	0.09
pole	0.08	0.05	0.06	0.21	0.05	0.06
traffic-sign	0.04	0.04	0.02	0.13	0.02	0.08
CovGap	0.39	0.06	0.06	0.53	0.04	0.05
AvgSize	4.66	0.62	0.42	5.22	0.25	0.17